Persistent Future North Atlantic Tropical Cyclone Risk in Two Contrasting CMIP6 Scenarios

Ratnaksha Lele[1], Adam H. Sobel[1,2], Chia-Ying Lee[1], Suzana J. Camargo[1,3], Patrick Kelly[4], Ted Amdur[5], Radovan Drinka[5]

[1]Lamont-Doherty Earth Observatory, Columbia University, Palisades, NY
[2]Department of Applied Physics and Applied Mathematics, Columbia University, New York, NY
[3]Columbia Climate School, Columbia University, New York, NY
[4]Aon Climate Risk Advisory, USA
[5]Aon Impact Forecasting, Chicago, IL

Key Points:

- A statistical-dynamical downscaling model characterizes future North Atlantic TC activity under CMIP6 low and high forcing scenarios
- Regional North Atlantic TC trends show persistent risk under both scenarios despite different warming levels
- Future regional North Atlantic TC activity is more sensitive to SST warming pattern than to global mean change

Corresponding author: Ratnaksha Lele, `rlele@ldeo.columbia.edu`

Abstract

We analyze North Atlantic Tropical Cyclone (TC) activity using the Columbia HAZard (CHAZ) model to downscale 12 models from CMIP6 under the SSP1-2.6 and SSP5-8.5 scenarios — those with the least and greatest anthropogenic forcing respectively. TC frequency increases along the Southeastern U.S. and declines along the Gulf under both SSPs. Greater TC frequency is not projected in the highest-warming scenario (SSP5-8.5) than in the lowest-warming scenario (SSP1-2.6) in the North Atlantic basin, even though it is in the global mean. These patterns remain broadly consistent over the 21st century, with stronger changes under higher-emission scenarios. The response appears driven primarily by El Niño-like shifts in the tropical Pacific mean state that influence Atlantic potential intensity and vertical wind shear. These results suggest that regional TC activity is more sensitive to the pattern of surface warming than to its global mean, and highlight the importance of the tropical Pacific in particular.

Plain Language Summary

Tropical cyclones (TCs) cause major damage along the U.S. coastline, and understanding how TC risk may change in the future is an important consideration for climate adaptation. We used a tropical cyclone risk modeling framework driven by simulations from 12 global climate models to examine how storm landfalls in the North Atlantic might change under both low and high greenhouse gas (GHG) emission scenarios. The results show a clear regional contrast: storms become more frequent along the Southeastern U.S. coast but less frequent along the Gulf Coast, including Texas. This pattern appears in both future climate scenarios and becomes stronger later in the century. The Atlantic TC changes are linked to patterns of change in oceanic and atmospheric conditions that resemble those often seen during El Niño events, and are consistent with trends towards a long-term mean state that in some respects resembles El Niño that are present in the climate model simulations (but not in observations). Our results suggest that changes in regional TC risk depend less on the overall amount of warming than on the pattern, and that the pattern of tropical Pacific climate change is particularly important to North Atlantic TC activity and U.S. TC risk.

1 Introduction

Tropical cyclones (TCs) are among the most damaging natural hazards on Earth, producing widespread societal and economic impacts globally, especially in coastal regions. Understanding the present-day TC hazard risk and how it may evolve under anthropogenic climate change remains a key challenge for the scientific community (Broccoli & Manabe, 1990; Bengtsson et al., 1996; Landsea et al., 1999; Knutson et al., 2010; Sobel et al., 2016; Walsh et al., 2016; Knutson et al., 2020; Camargo et al., 2023). Along with analysis of the observational record, process-based understanding is essential to meeting this challenge.

TC activity is controlled by a combination of environmental factors including potential intensity (PI), vertical wind shear, mid-tropospheric humidity, and large-scale vorticity (Gray, 1968, 1984; Emanuel, 1987; Camargo, Sobel, et al., 2007; Sobel et al., 2016), which in turn are themselves shaped by large-scale circulation patterns and sea surface temperature (SST) distributions. Changes in the location of preferred genesis regions can modify track distributions (B. Wang & Chan, 2002; Camargo, Robertson, et al., 2007; Daloz et al., 2015), while alterations in large-scale steering flows can shift storm translation direction and speed (Chan, 2005; Colbert et al., 2013). These dynamical responses can lead to substantial regional changes in TC hazard by redistributing TC activity within basins (Jones & Thorncroft, 1998; Saunders et al., 2000; Murakami & Wang, 2010; Yokoi et al., 2013; Nakamura et al., 2017).

Assessments of tropical cyclones' response to climate change have tended to focus on global-scale aspects. At global scales, for example, there is relatively high confidence that TC intensifies the strongest storms with warming (e.g. Knutson et al. (2015); Yoshida et al. (2017); Knutson et al. (2020)), while on the other hand projections of TC frequency remain highly uncertain (Knutson et al., 2010; Walsh et al., 2016; K. A. Emanuel, 2013; Zhao et al., 2026; Vecchi et al., 2019; Sobel et al., 2021; Camargo et al., 2023; Chavas et al., 2025). A focus on global-scale changes could potentially bias regional hazard and risk assessments, if the global-scale changes are assumed to apply directly at local scales (e.g. Jewson (2024)). For some climate hazards, such as heat for example, this may be appropriate, because global and regional changes tend to have at least the same signs, if not also similar magnitudes. Some other aspects of climate may exhibit changes that vary spatially in both sign and magnitude, e.g., whose magnitudes at a given location scale with global mean surface temperature. In this study, we present results which suggest that neither is true of tropical cyclone hazard. For tropical cyclones, changes on basin and sub-basin scales can be larger than those at global scales, and both may depend much more on the pattern of surface warming than on its global mean.

We use the Columbia HAZard (CHAZ) model (Lee et al., 2018), a statistical–dynamical framework which has been previously used to downscale simulations from Coupled Model Intercomparison Project (CMIP) simulations to project changes in global and regional TC activity (e.g. Lee et al. (2020); Fosu et al. (2024)), as well as to economic losses from landfalling TCs (Meiler et al., 2022; Baldwin et al., 2023). CHAZ is one of a class of statistical–dynamical downscaling models (e.g. K. A. Emanuel et al. (2008); Lee et al. (2018); Bloemendaal et al. (2020); Jing and Lin (2020)), that synthesize large catalogs of physically consistent synthetic TCs using environmental fields from CMIP-class models or reanalysis data sets. This approach generates the large event sets needed for probabilistic risk analysis, including rare extreme events (Meiler et al., 2022; Baldwin et al., 2023; Fosu et al., 2024; Hemmati et al., 2025; Meiler et al., 2026), at lower cost than regional dynamical downscaling (Knutson et al., 2013; Patricola et al., 2017; Fu et al., 2019) or variable-resolution GCMs (Zarzycki et al., 2014; Stansfield et al., 2020).

We extend the CHAZ-based analysis of North Atlantic TC risk of Fosu et al. (2024), who downscaled 12 CMIP6 models (Eyring et al., 2016) under the SSP2-4.5, SSP3-7.0, and SSP5-8.5 scenarios, by adding the low-emissions SSP1-2.6 scenario. This enables comparison between the two extreme ends of the emissions spectrum (SSP1-2.6 and SSP5-8.5), and allows us to more fully explore the sensitivity of U.S. TC hazard risk to the degree of warming. For reference, end-of-century (2080-2100) global mean temperature change relative to the 1995-2014 baseline is expected to be in the range of 1.23 ± 0.83°C for SSP1-2.6 and 3.99 ± 1.59°C for SSP5-8.5 (Riahi et al., 2017; Tebaldi et al., 2021). Our specific objectives are to: (1) project changes in North Atlantic TC genesis, tracks, and intensity; (2) quantify the evolving hazard of landfalling TCs to the U.S. coast; and (3) identify the factors that drive regional differences in projected North Atlantic TC risk. By linking projected North Atlantic TC activity to the spatial structure of environmental change in CMIP6 models, this study highlights the role of the pattern of warming, rather than just its magnitude, in shaping future regional TC activity and hazard.

The paper is structured as follows. Section 2 describes the CHAZ model, the CMIP6 data and bias correction, and the analysis methodology. In Section 3 we present our main finding as they relate to changes in landfalling frequency focused on the North Atlantic basin, followed by a discussion in Section 4 on the role of spatial patterns in the model's large scale environmental fields shape the emergent TC risks in the basin in both SSP scenarios.

2 Data and Methods

2.1 Downscaling CMIP6 Data with Columbia HAZard Model (CHAZ)

The Columbia HAZard model (CHAZ; (Lee et al., 2018)) is a statistical-dynamical downscaling model designed to establish a physical link between large-scale climate drivers of TC activity. Informed by background environmental forcing from climate model or observational reanalysis output, CHAZ is designed to simulate TC tracks, and consists of three distinct components that simulate storm genesis, track, and intensity.

The genesis component generates weak disturbances at a rate determined by environmental conditions, calculated using the Tropical Cyclone Genesis Index (TCGI) of Tippett et al. (2011) as modified by Camargo et al. (2014). The seeding rate, μ_{MV}, is given by:

$$\mu_{MV} = \exp(b + b_\eta \eta_{850} + b_{MV} MV + b_{PI} PI + b_{Vshear} Vshear) \quad (1)$$

where the moisture variable (MV) is either column relative humidity (CRH) or saturation deficit (SD), following (Lee et al., 2020). Note that we only discuss results from TCGI calculated using CRH in this study. The CRH version of CHAZ is the one that leads to increases in global TC frequency, thus greater hazard and risk; more importantly, our focus here is on the patterns of change, which are similar in the SD version, just with overall decreases. The coefficients b are constants, η_{850} is the 850 hPa absolute vorticity, PI is the potential intensity (Bister & Emanuel, 2002), and $Vshear$ is the deep layer vertical wind shear (850–250 hPa), calculated as the magnitude of difference in vector winds between the two pressure levels.

The coefficients for the TCGI used in this study have been updated from (Lee et al., 2018) and are derived from a Poisson regression using environmental fields from the fifth generation of the European Centre for Medium-Range Weather Forecasts (ECMWF) global atmospheric reanalysis (ERA5) (Hersbach et al., 2020) over the period 1981–2010, as described in Camargo et al. (2025). For TCGI-CRH, the coefficients are $b = -24.132$, $b_\eta = 2.512$, $b_{CRH} = 0.077$, $b_{PI} = 0.062$, and $b_{Vshear} = -0.120$. Further, following Camargo et al. (2025); Fosu et al. (2024), environmental predictors downscaled from CMIP6 (Eyring et al., 2016) used in the genesis component of the model, were bias-corrected by adjusting the monthly historical model climatology to match the ERA5 reanalysis climatology for the period 1981–2010, with the assumption of time-invariant biases applied to the CMIP6 future scenarios SSP1-2.6 and SSP5-8.5 (O'Neill et al., 2017) for years 2015 to 2100.

The track component of the model is based on a beta and advection model that moves storms via advection by a monthly mean environmental wind (defined as a weighted mean of a low-level [850 hPa] and an upper-tropospheric level [250 hPa]) along with a beta drift component (Emanuel et al., 2006), and a stochastic component based on eddy statistics to account for sub-monthly wind fluctuations. The intensity component is based on a multiple linear regression on key environmental parameters, with an auto-regressive stochastic error term to account for internal storm dynamics (Lee et al., 2015, 2016, 2018). A separate multiple linear regression model estimates intensity decay during and post-landfall (Lee et al., 2015, 2018). Since environmental predictors in the CHAZ's intensity module are normalized by the model's tropical mean, additional bias-correction as applied to TCGI predictors is not applied to the track and intensity predictor variables.

We downscaled CHAZ using output from 12 models that participated in CMIP6 (Eyring et al., 2016), as listed in Table 4. We utilized simulations from the historical scenario (HIST, 1951–2014; [from Fosu et al. (2024)]) and two future scenarios: the low-emissions scenario SSP1-2.6 (SSP126) and the high-emissions scenario SSP5-8.5 (SSP585) [from Fosu et al. (2024)] O'Neill et al. (2017), both covering the period 2015–2100. While the downscaling was performed globally, this analysis focuses exclusively on TC activity in the North Atlantic basin (ATL, 0–55°N, 100–20°W).

For each CMIP6 model and scenario (HIST, SSP126, SSP585), we downscaled a single ensemble member as indicated in Table 1. For each of these runs, we applied 10 realizations of the random seeding process, each with 40 realizations of the stochastic intensity model, generating 400 unique synthetic TC event sets per model and scenario. This resulted in 25,600 synthetic years for the historical period (64 years × 400 combinations) and 34,400 synthetic years for the future period (86 years × 400 combinations) for each of the 12 models. For the North Atlantic basin, the historical period (1951-2014) dataset consists of a total of 122474 storms, while the future (2015-2100) SSP1-2.6 and SSP5-8.5 dataset contains 192048 and 189390 total storms respectively, a sample size necessary for robust probabilistic risk assessment (Lin & Emanuel, 2016). The synthetic track dataset include storm position (longitude, latitude) and maximum sustained wind speed (kt) at six-hour intervals.

2.2 Estimating Changes to TC Landfall Hazard

To analyze landfall hazard, we defined seven landfall "gates" along the U.S. Atlantic and Gulf coastlines (Supporting Information, Figure S1). The coastline data were obtained from the Natural Earth physical vector dataset (Kelso & Patterson, 2010). A landfall event was identified when a synthetic TC track intersected a coastline segment within a defined gate.

To provide a compact representation of the typical tracks associated with landfalling storms in each coastal gate, we construct an average composite track from tracks across all models and track ensembles intersecting the defined coastal gate during the the historical (1951-2014) simulation period (Figure 3, tan solid). For each storm that crosses a given gate, the time of gate crossing is defined as *t=0*, and the corresponding storm is retained for analysis. To characterize the typical approach pathway of the landfalling storms for the respective gate, all TC trajectories are temporally aligned relative to their individual gate-crossing time. The segment of the track extending backwards up to 10 days (a total of 40, 6-hourly time steps) prior to landfall is extracted for the storm. When a storm's lifetime does not span the full 10-day window, the available portion of the track is retained and earlier times are padded, allowing all storms to contribute without imposing equal-length constraints. A 10-day composite average track is then constructed by averaging storm positions at each relative time step across all storms. This then yields a set of latitude–longitude points (composite track) that trace the most probable pathway of storms contributing to landfall in that gate, capturing the central tendency of storm motion associated with each gate and provides a useful diagnostic for comparing how environmental changes along these preferred pathways influence regional landfall risk (Figure 4, black solid). While previous studies have applied unsupervised learning techniques—such as K-means clustering (Elsner, 2003), mass moments (Nakamura et al., 2009), or mixture models (Kossin et al., 2010)—to classify tropical cyclone track pathways, these approaches are not required here. In our framework, the predefined coastal gates inherently partition the track dataset, effectively delineating pathway groupings a priori. As a result, we directly compute composite-average landfall tracks for each gate, yielding an equivalent classification without the need for additional clustering methods. .

Our analysis of the historical period focuses on the 1951–2014 era, while for future projections (SSP1-2.6 and SSP5-8.5), we analyze three 20-year epochs: early-century (2030–2050), mid-century (2060–2080), and late-century (2080–2100).To evaluate the model's historical performance, we compared CHAZ downscaled data against the observed TC record from the International Best Track Archive for Climate Stewardship (IBTrACS; (Knapp et al., 2010, 2018)). We used version v04 of the dataset, which for the North Atlantic basin uses tracks provided by National Hurricane Center.

To quantify the evolving TC hazard, we computed annual landfall frequencies and return periods for different intensity thresholds at each gate based on the Saffir-Simpson

wind scale. The annual frequency of exceedance for a given landfall wind speed threshold is the probability of one or more TCs making landfall with an intensity greater than that threshold in a given year. The return period (in years) for wind speeds exceeding this threshold is then calculated as the inverse of this annual exceedance probability (AEP) for the corresponding gate.

We assess the change in hazard due to anthropogenic climate change using a "climate change delta" (cc-delta) approach (Fosu et al., 2024). The cc-delta for a specific TC statistic (e.g., landfall frequency of major hurricanes) is calculated as the difference between the future epoch mean and the historical period mean, normalized by the historical mean to express a percentage change:

$$\text{cc-delta} = \frac{\overline{X}_{\text{future}} - \overline{X}_{\text{historical}}}{\overline{X}_{\text{historical}}} \times 100\% \tag{2}$$

The mean values are calculated across the 12-model ensemble, with each model represented by the mean of its 400 realizations. To assess statistical significance, we applied a two-sided Student's t-test to the ensemble of model means (n=12) for historical and future periods, with a p-value of 0.05 serving as the significance threshold.

3 Results

3.1 Changes to Landfalling TC Risk

Figure 1 shows the multi-model mean change in North Atlantic tropical cyclone (TC) track density between the future (2015–2100) and historical (1951–2014) periods for SSP1-2.6 and SSP5-8.5. While basin-scale changes are spatially heterogeneous, a coherent and persistent regional signal emerges along the U.S. coastline. In particular, TC activity (including non-landfalling storms) decreases along much of the Gulf coastline, including the Texas region, while increasing along the Southeastern U.S. coast under both forcing scenarios. These patterns are evident throughout the 21st century and are amplified under the higher-emissions SSP5-8.5 scenario (Figure 1, Supporting Information Figure S2).

Changes in landfalling TC frequency at the regional scale are quantified in Figure 2 using the Texas and Southeast coastal gates. Across all three future periods (near-term, mid-century, and late century), the Texas gate exhibits a trend towards a reduction in TC frequency relative to the historical baseline under both SSP1-2.6 and SSP5-8.5 (Figures 2a,b), with marginal increases in the near-term (2030-2050) to significant decline across all storm categories especially in SSP5-8.5 . The magnitude of the decrease grows with time and is consistently larger under SSP5-8.5. Ensemble-mean return period curves shift toward longer return periods for frequent events, indicating a reduced likelihood of TC landfalls in the Texas region despite increasing inter-model spread (Figure 2e,f).

In contrast, the Southeast gate shows an increase in landfalling TC frequency under both scenarios (Figure 2 c,d). This increase is detectable as early as the near-term period (2030-2050) and strengthens toward the late 21st century (2080-2100), particularly under SSP5-8.5. Ensemble-mean return periods slightly shorten relative to the historical climate, implying an increased probability of TC landfalls along the Southeast US coastline (Figure 2g,h). The opposing responses between the Texas and Southeast gates persist across scenarios.

These contrasting regional responses indicate that future TC risk along the U.S. coastline is neither spatially uniform, nor monotonically related to greenhouse gas forcing. Instead, changes in landfall frequency depend strongly on location, with the Gulf Coast and Southeast responding in opposite directions under both low- and high-emissions pathways.

3.2 Basin-Scale Environmental Drivers of Regional TC Risk

To investigate the physical mechanisms underlying the contrasting regional landfall responses, Figures 3 and 4 examine basin-wide TC track behavior together with changes in the large-scale environmental fields that determine that behavior in CHAZ. Figure 3 shows the average TC track density for storms making landfall in the Texas and Southeast gates. Texas-landfalling storms preferentially originate and traverse the western Atlantic and Caribbean, while Southeast-landfalling storms are more strongly associated with genesis and propagation across the central and eastern Main Development Region (MDR) defined between 10°–20°N latitude, and 20°–85°W longitude. These distinct pathway differences suggest that regional landfall changes may be linked to spatially varying environmental conditions along the dominant storm tracks.

Here, we focus on basin-wide changes in late-century changes in potential intensity (PI) normalized by global mean temperature change, vertical wind shear (850–250 hPa), and steering flow for SSP1-2.6 and SSP5-8.5. Changes in PI are scaled by the corresponding change in global-mean surface air temperature (ΔT) to obtain a per-degree warming response. The change in global-mean surface air temperature is computed for each model as the area-weighted global-mean annual-mean surface air temperature, averaged over the future (here, 2080-2100) and historical (1951-2014) periods, and the differences between the two. Changes in PI are then normalized by ΔT on a per-model basis to obtain dPI/dT, which is subsequently averaged across all models for each scenario. This PI pattern change in the Atlantic is very robust and present in multiple versions of CMIP (e.g. Vecchi and Soden (2007a); Camargo (2013); Ting et al. (2015); Sobel et al. (2016); Camargo et al. (2025)).

Across both scenarios, vertical wind shear increases over the western Atlantic, Gulf of Mexico, and Caribbean (western MDR), while weakening across portions of the central and eastern MDR (Figure 4 c,d)). This pattern is known to be present across future scenarios in past and current CMIP versions (e.g. Vecchi and Soden (2007a); Camargo (2013); Sobel et al. (2016); Ting et al. (2019); Camargo et al. (2025)). The representative tracks for Texas-landfalling storms intersect regions of enhanced shear, whereas Southeast-landfalling tracks pass through regions of reduced shear. This spatial contrast is more pronounced under SSP5-8.5, consistent with the larger magnitude changes in landfall frequency seen in Figure 2. We find that the reduced deep-layer (850–250 hPa) vertical wind shear in the central MDR and western North Atlantic basin creates a more favorable dynamical environment for storms ultimately tracking towards the Southeast coast, increases landfalling TC risk in the Southeast preferentially towards stronger and more intense storm categories (Figure 2 c,d). Changes in PI exhibit a broadly positive signal across much of the tropical Atlantic, indicating an overall thermodynamic environment more favorable for TC intensification. PI increases are broadly distributed across the basin, with comparatively modest spatial structure, including a local minimum in the MDR in both SSPs (Figure 4a,b). While enhanced PI may support increased TC hazard in both the coastal regions of the Southeast and Texas, the shear signal is more directly consistent with the contrasting responses in landfall risk between the two regions (Figure 2 a,b versus c,d).

TC motion is largely governed by the surrounding deep-layer synoptic-scale flow structure (Chan & Gray, 1982; Holland, 1983; Chan, 2005). Regardless of the emission scenario considered here, we find that shifts in large-scale atmospheric steering winds alter storm tracks and forward speeds, ultimately leading to changes the landfall risk for different coastal regions. The projected changes in steering flow (Figure 4e,f) exhibit a coherent basin-scale pattern characterized by enhanced easterly flow across the tropical Atlantic and Caribbean. While the magnitude of the anomalies is more pronounced under SSP5-8.5, the overall structure in the vector winds is consistent between between SSP1-2.6 and SSP5-8.5. The resulting steering anomalies in both direction and magnitude tend to favor storm propagation across the central MDR towards the western North

Atlantic basin and the Southeast U.S. coastline, while reducing the likelihood of westward tracking storms to find favorable steering patterns within the western Caribbean and Gulf of Mexico. In combination with the spatial distribution of vertical wind shear and PI anomalies, these circulation changes reinforce the divergence in regional TC risk between the two coastlines by influencing the movement and tracking of storms in the basin (Figure 4c).

The combined PI and shear patterns resemble an El Niño–like response in the large-scale climate system, characterized by increased vertical wind shear over the western Atlantic and reduced shear across the central MDR (Gray, 1984; Goldenberg & Shapiro, 1996; Aiyyer & Thorncroft, 2006; Vecchi & Soden, 2007b). Such a pattern is known to suppress Atlantic TC activity in regions influenced by stronger shear while favoring genesis and intensification where shear is reduced (Gray, 1984; Patricola et al., 2014; Tang & Neelin, 2004; Klotzbach, 2011; Rios-Berrios et al., 2024). In this framework, the El Niño–like forced response preferentially enhances TC activity along Southeast-oriented pathways while suppressing activity for storms tracking toward the Gulf Coast.

Together, these results indicate that forced changes in basin-scale environmental fields—particularly vertical wind shear—play a central role in shaping the regional redistribution of landfalling TC risk. The persistence of these patterns across SSP1-2.6 and SSP5-8.5 suggests that regional TC risk along the U.S. is more sensitive to large-scale circulation changes than to the degree of global warming per se.

4 Discussion and Conclusions

This study identifies a robust, forced redistribution of North Atlantic tropical cyclone landfall risk along the U.S. coastline under both low- and high-emissions scenarios. Using simulations with a statistical-dynamical downscaling model driven by 12 Earth system models from CMIP6 (Table 4), we find a consistent decrease in landfalling TC frequency in the Gulf of Mexico, particularly the Texas coastline, alongside an increase along the Southeastern U.S. coast (Figure 2 a-d). These opposing regional responses persist across SSP1-2.6 and SSP5-8.5, differing primarily in magnitude rather than sign. This indicates that mitigation pathway alone does not determine the spatial pattern of future TC risk, underscoring the importance of regional-scale assessment for adaptation planning.

The contrasting landfall responses appear closely linked to basin-wide changes in large-scale environmental conditions that influence TC genesis, intensification, and steering. In particular, changes in vertical wind shear emerge as a dominant factor shaping regional outcomes. Storms that ultimately make landfall along the Southeast preferentially traverse regions where vertical wind shear weakens in the future climate, enhancing TC favorability. In contrast, Texas- and Gulf Coast–bound storms encounter regions of increased shear, which likely suppress TC development and survival. While potential intensity generally increases across much of the tropical Atlantic, its spatial gradients are comparatively weak and do not offset the strongly regional nature of the shear response. While these basin-scale patterns of change in PI and vertical wind shear are consistent with results from previous CMIP3 (Vecchi & Soden, 2007a, 2007b) and CMIP5 models (Camargo, 2013; Ting et al., 2015, 2019; Sobel et al., 2016), as well as CMIP6 models (Camargo et al., 2025), here we demonstrate their linkage to regional differences in landfalling TC activity for the North Atlantic basin.

The spatial structure of the projected environmental changes over the Atlantic, particularly the increase in vertical shear over the western Atlantic, resembles those associated with El Niño events. This suggests that these shear changes are associated with the broadly El Niño-like pattern of change in the tropical Pacific SST trends in the models, characterized by weakened zonal SST gradients. On interannual timescales, the ver-

tical shear anomalies play an important role in modulating North Atlantic TC activity (Gray, 1984; Goldenberg & Shapiro, 1996; Klotzbach, 2011; Patricola et al., 2014; Smith et al., 2007; Pielke & Landsea, 1999; Kossin et al., 2010). Our results suggest that analogous circulation changes arise as part of the forced climate response, effectively imprinting an El Niño-like trend onto the pattern of Atlantic TC activity. This pattern strengthens with warming, such that TC hazard along the Gulf coast is more suppressed in SSP5-8.5 than in SSP1-2.6, even as TC hazard increases more in SSP5-8.5 than in SSP1-2.6 along the Atlantic coast of the southeast US. Southeast-favoring storm tracks increasingly align with regions of reduced shear, while Gulf-oriented tracks encounter increased shear, producing the divergent landfall trends identified in this study.

Several limitations warrant consideration. Our analysis focuses on landfalling TC frequency rather than intensity, rainfall, or compound hazards, which may respond differently to environmental forcing. While the CHAZ framework captures key large-scale controls on TC activity, the robustness of the El-Niño–like mean-state response in CMIP6 projections remains an active area of inquiry. Recent work highlights observed trends over the historical period that are more similar in pattern to La Niña than to El Niño, with cooling in the eastern Equatorial Pacific and strengthened zonal gradients, in strong contrast to simulations (Seager et al., 2019, 2022; Wills et al., 2022; Zhuo et al., 2025). Models also disagree in projected ENSO characteristics with no clear consensus on future changes in ENSO frequency, amplitude structure (e.g. C. Wang et al. (2017); Cai et al. (2021); Erickson and Patricola (2023); Zhuo et al. (2025)). Consequently, while the ENSO-like circulation pattern provides a useful dynamical framework for interpreting the environmental changes identified here, the degree to which the pattern of TC hazard identified in the simulations here will emerge in the real climate system remains highly uncertain. On the other hand, the broader conclusion is that the pattern of SST change is more important than the global mean warming to regional TC hazard and risk. This might well remain true even if the sign of the pattern change were reversed, and thus is, in our view, more likely to be a robust conclusion. Furthermore, the inferred *cc-delta* signal depends on the baseline distribution of TC genesis and track pathways in the model. If the models exhibit specific regional biases which differ from the observed TC regional climatology, the resulting deltas could be biased too. While a bias-correction is applied to match the observed frequency of landfalling storms within each coastal gate, residual biases in the spatial distribution of genesis and track pathways may still influence the magnitude of the projected changes.

These findings also highlight that future TC risk cannot be inferred solely from basin-wide metrics such as total TC frequency or mean intensity. Changes in large-scale circulation patterns can reorganize where storms preferentially form, intensify, and move, leading to persistent regional contrasts in landfall risk even when the overall basin response is muted or uncertain (Knutson et al., 2020; Sobel et al., 2021; Camargo et al., 2023). The persistence of the Gulf-Atlantic TC hazard contrast across emissions scenarios suggests that internal variability and regional circulation responses may exert a stronger control on future landfall risk than the magnitude of warming or emissions pathways alone. Future work should examine how internal climate variability, including from combined effects of ENSO and Atlantic Multi-decadal Oscillation and their modulation under warming, may interact with the forced response identified here to influence decadal-scale fluctuations in regional TC risk.

In summary, our results demonstrate that regional TC landfall risk along the U.S. coastline is highly sensitive to large-scale circulation changes under climate change. The opposing responses between the Gulf Coast and Southeast persist even under strong mitigation, emphasizing that adaptation strategies must account for geographically specific risk trajectories rather than relying on basin-wide projections alone.

Availability Statement

The IBTrACS dataset can be downloaded from `https://www.ncei.noaa.gov/products/international-best-track-archive`. The publicly available CMIP6 multi-model ensemble dataset was used in this paper. CMIP6 ensemble model outputs can be downloaded from the different Earth System Grid Federation (ESGF) nodes. CHAZ is an open-source model and can be downloaded from `https://github.com/cl3225/CHAZ`.

Acknowledgments

RL, AHS, SJC, and CYL acknowledge funding support for this work by Aon plc.

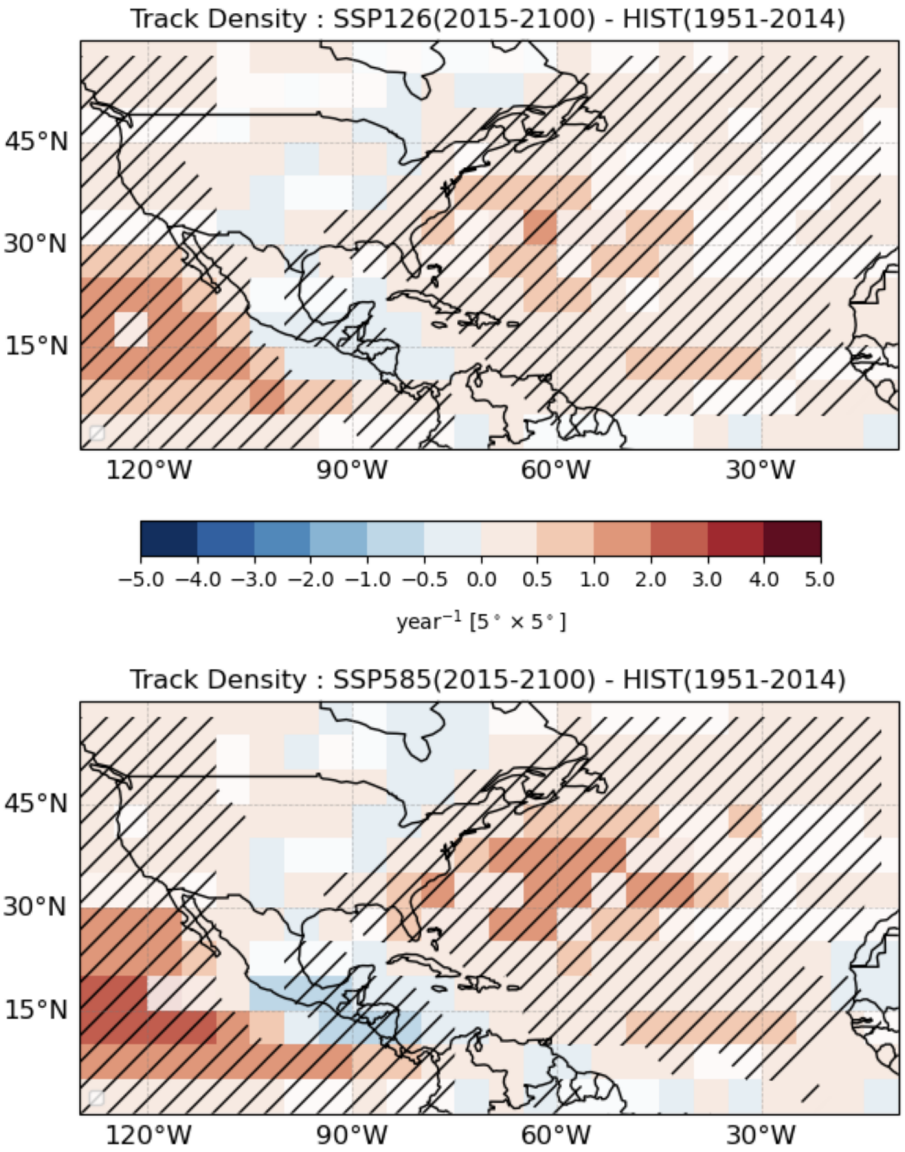

Figure 1. Multi-Model Mean of track density change in the North Atlantic, calculated between future (2015-2100) and historical (1951-2014) periods for SSP126 (top) and SSP 585 (bottom). The density changes are calculated from the 12 CMIP6 model outputs each with 10 track ensemble members (see Section 2). Stippling shows regions with statistically significant differences at p = 0.05 based on a two-sided student's t-test from the 12-model, 10-track and 40-member intensity ensemble.

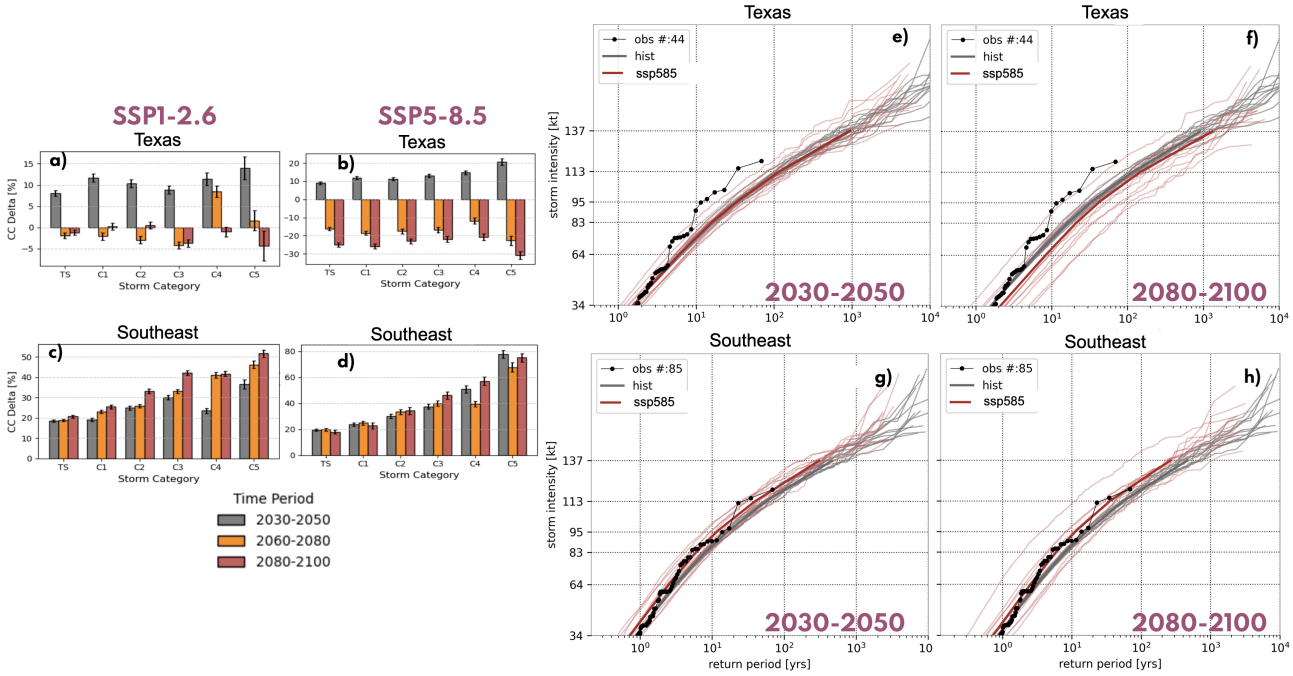

Figure 2. Change in TC frequency due to climate change (cc-delta) for SSP126 and SSP585 in the Texas (a,b) and Southeast Gates (c,d) for near-term (2030-2050), mid-century (2060-2080) and late century (2080-2100) time periods. Modeled return periods for the near-term and late century (thin red), historical period (thin gray) for SSP5-8.5 and IBTrACS observations (solid black), along with ensemble means (thick solid) calculated from each of the 12 CMIP6 models are shown for Texas (e,f) and Southeast (g,h) gates.

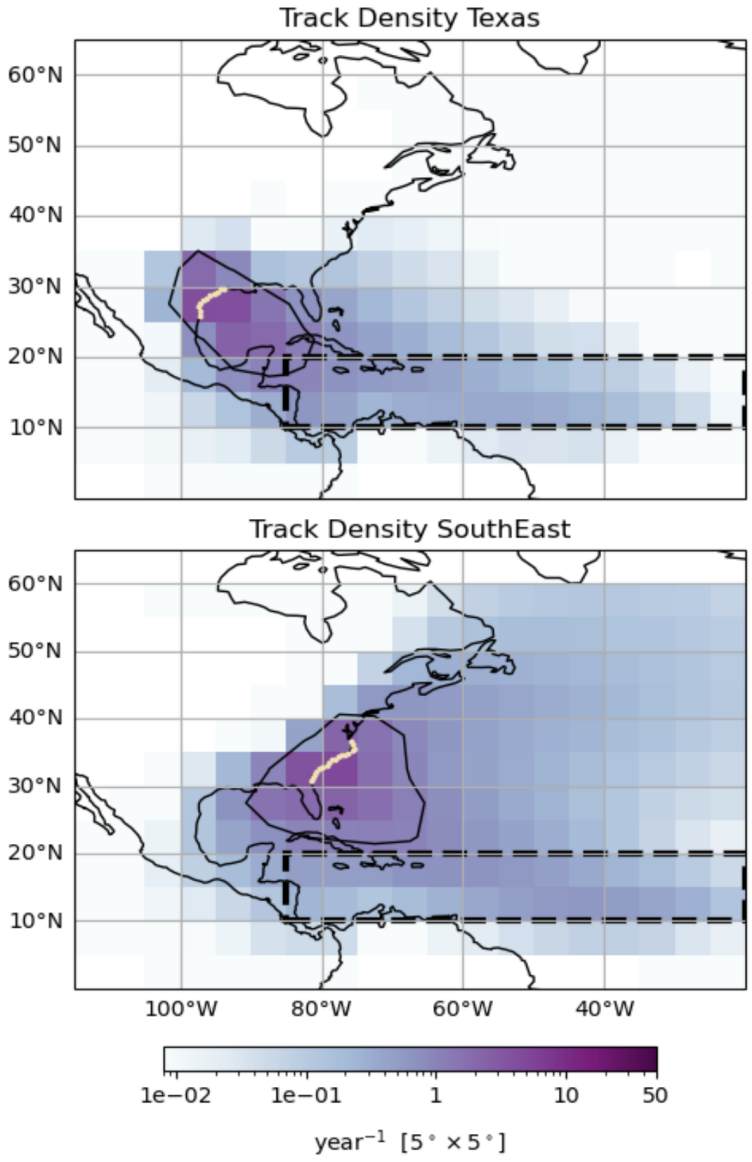

Figure 3. Average track density (year^{-1}) computed on a 5^o $\times 5^o$ grid for tracks landfalling within the Texas (top) and SouthEast (bottom) gates calculated using the 12 CMIP6 model data simulated by CHAZ's, 10 seed and 40 ensemble-member track set for the historical period (1951-2014). The Atlantic MDR (dashed black), the location of the coastal gate (tan solid), and delineation for 1 storm per year (solid black contour) is shown for reference.

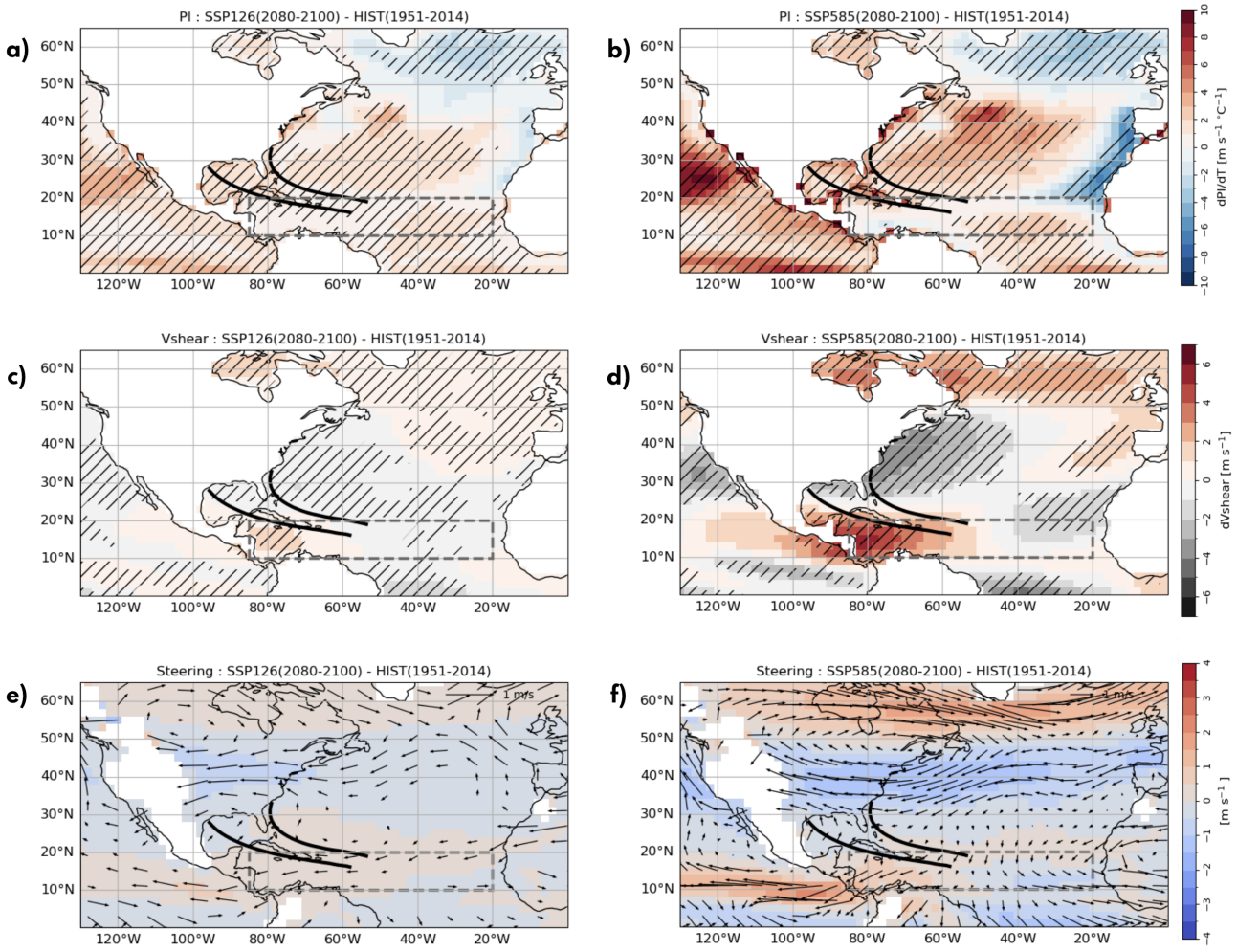

Figure 4. The multi-model mean difference between the late-century (2080-2100) and historical (1951-2014) time period for PI change per degree of warming (dPI dT^{-1}) [a,b], 850-250 hPa vertical wind shear (m s^{-1}) [c,d], and mean steering flow (m s^{-1}) [e,f] for SSP1-2.6 and SSP5-8.5 (top and bottom respectively). Differences shown are calculated for August-October in the Northern Hemisphere. The average 10-day composite storm track for TCs landfalling within the Texas and Southeast gates, calculated 10 days prior to landfall using all storm tracks that made landfall within each gate (see Section 2.2) is also indicated (solid black), along with the Atlantic MDR (dashed black). Stippling indicates regions where atleast 75% of models agree on the sign of the ensemble mean change.

Table 1. The CMIP6 models downscaled for SSP1-2.6 and SSP5-8.5 scenarios in the study.

Institution	Model	Downscaled member	Model Resolution	Reference
CSIRO	ACCESS-ESM1-5	r3i1p1f1	250 km	Ziehn et al. (2020)
NCAR	CESM2	r4i1p1f1	100 km	Danabasoglu et al. (2020)
CNRM & CERFACS	CNRM-CM6-1	r2i1p1f2	250 km	Voldoire et al. (2019)
EC-Earth Consortium	EC-Earth3	r1i1p1f1	100 km	Döscher et al. (2022)
NOAA-GFDL	GFDL-ESM4	r1i1p1f1	100 km	Dunne et al. (2020)
NASA-GISS	GISS-E2-1-G	r1i1p1f2	250 km	Kelley et al. (2020)
MOHC	HadGEM3-GC31-LL	r1i1p1f3	250 km	Williams et al. (2021)
IPSL	IPSL-CM6A-LR	r1i1p1f1	250 km	Boucher et al. (2020)
MIROC Consortium	MIROC6	r1i1p1f1	250 km	Tatebe et al. (2019)
Max Planck Institute	MPI-ESM1-2-HR	r1i1p1f1	100 km	Müller et al. (2018)
MRI	MRI-ESM-2-0	r1i1p1f1	100 km	Yukimoto et al. (2019)
UK Met Office	UKESM1-0-LL	r1i1p1f2	250 km	Sellar et al. (2019)

[a] All models are part of the CMIP6 ensemble.

References

Aiyyer, A., & Thorncroft, C. (2006). Climatology of vertical wind shear over the tropical Atlantic. *Journal of Climate*, *19*(12), 2969–2983. doi: 10.1175/JCLI3685.1

Baldwin, J. W., Lee, C.-Y., Walsh, B. J., Camargo, S. J., & Sobel, A. H. (2023). Vulnerability in a tropical cyclone risk model: Philippines case study. *Weather, Climate, and Society*, *15*, 503–523. doi: 10.1175/WCAS-D-22-0049.1

Bengtsson, L., Botzet, M., & Esch, M. (1996). Will greenhouse gas-induced warming over the next 50 years lead to higher frequency and greater intensity of hurricanes? *Tellus A*, *48*(1), 57-73. doi: https://doi.org/10.1034/j.1600-0870.1996.00004.x

Bister, M., & Emanuel, K. A. (2002). Low frequency variability of tropical cyclone potential intensity 1. interannual to interdecadal variability. *Journal of Geophysical Research: Atmospheres*, *107*(D22), 4621. doi: 10.1029/2001JD000780

Bloemendaal, N., Haigh, I. D., de Moel, H., Muis, S., Haarsma, R. J., & Aerts, J. C. J. H. (2020). Generation of a global synthetic tropical cyclone hazard dataset using STORM. *Scientific Data*, *7*, 40. doi: 10.1038/s41597-020-0381-2

Boucher, O., et al. (2020). Presentation and evaluation of the IPSL-CM6A-LR climate model. *Journal of Advances in Modeling Earth Systems*, *12*, e2019MS002010. doi: 10.1029/2019MS002010

Broccoli, A. J., & Manabe, S. (1990). Can existing climate models be used to study anthropogenic changes in tropical cyclone climate? *Geophysical Research Letters*, *17*(11), 1917-1920. doi: https://doi.org/10.1029/GL017i011p01917

Cai, W., Santoso, A., Collins, M., Dewitte, B., Karamperidou, C., Kug, J.-S., ... Zhong, W. (2021, September). Changing El Niño–Southern Oscillation in a warming climate. *Nature Reviews Earth and Environment*, *2*(9), 628–644. (Published online: 17 August 2021) doi: 10.1038/s43017-021-00199-z

Camargo, S. J. (2013). Global and regional aspects of tropical cyclone activity in the CMIP5 models. *Journal of Climate*, *26*, 9880–9902. doi: 10.1175/JCLI-D-12-00549.1

Camargo, S. J., et al. (2023). An update on the influence of natural climate variability and anthropogenic climate change on tropical cyclones. *Tropical Cyclone Research and Review*, *12*, 216–239. doi: 10.1016/j.tcrr.2023.10.001

Camargo, S. J., Robertson, A. W., Gaffney, S. J., Smyth, P., & Ghil, M. (2007, July 15). Cluster analysis of typhoon tracks. Part I: General properties. *Journal of Climate*, *20*(14), 3635–3653. (Print publication: 15 July 2007) doi: 10.1175/JCLI4188.1

Camargo, S. J., Sobel, A. H., Barnston, A. G., & Emanuel, K. A. (2007). Tropical cyclone genesis potential index in climate models. *Tellus A*, *59*, 428–443. doi: 10.1111/j.1600-0870.2007.00238.x

Camargo, S. J., Tippett, M. K., Sobel, A. H., Lee, C.-Y., Fosu, B., & Hodges, K. I. (2025). Tropical cyclones and associated environmental fields in CMIP6 models. *Journal of Climate*, *38*, 3877–3902. doi: 10.1175/JCLI-D-24-0629.1

Camargo, S. J., Tippett, M. K., Sobel, A. H., Vecchi, G. A., & Zhao, M. (2014). Testing the performance of tropical cyclone genesis indices in future climates using the HiRAM model. *Journal of Climate*, *27*, 9171–9196. doi: 10.1175/JCLI-D-13-00505.1

Chan, J. C. L. (2005). The physics of tropical cyclone motion. *Annual Review of Fluid Mechanics*, *37*, 99–128. doi: 10.1146/annurev.fluid.37.061903.175702

Chan, J. C. L., & Gray, W. M. (1982, October 1). Tropical cyclone movement and surrounding flow relationships. *Monthly Weather Review*, *110*(10), 1354–1374. (Print publication: 1 October 1982) doi: 10.1175/1520-0493(1982)110⟨1354:TCMASF⟩2.0.CO;2

Chavas, D. R., Camargo, S. J., & Tippett, M. K. (2025). Tropical cyclone genesis potential using a ventilated potential intensity. *Journal of Climate*, *38*, 1667–1689. doi: 10.1175/JCLI-D-24-0186.1

Colbert, A. J., Soden, B. J., Vecchi, G. A., & Kirtman, B. P. (2013). The impact of anthropogenic climate change on North Atlantic tropical cyclone tracks. *Journal of Climate*, *26*(12), 4088–4104.

Daloz, A. S., et al. (2015). Cluster analysis of downscaled and explicitly simulated North Atlantic tropical cyclone tracks. *Journal of Climate*, *28*(4), 1333–1361. doi: 10.1175/JCLI-D-13-00646.1

Danabasoglu, G., et al. (2020). The community earth system model version 2 (CESM2). *Journal of Advances in Modeling Earth Systems*, *12*, e2019MS001916.

Dunne, J. P., et al. (2020). The GFDL earth system model version 4.1 (GFDL-ESM 4.1): Overall coupled model description and simulation characteristics. *Journal of Advances in Modeling Earth Systems*, *12*, e2019MS002015. doi: 10.1029/2019MS002015

Döscher, R., et al. (2022). The EC-Earth3 earth system model for the coupled model intercomparison project 6. *Geoscientific Model Development*, *15*, 2973–3020. doi: 10.5194/gmd-15-2973-2022

Elsner, J. B. (2003). Tracking hurricanes. *Bulletin of the American Meteorological Society*, *84*(3), 353–356. doi: 10.1175/BAMS-84-3-353

Emanuel. (1987). The dependence of hurricane intensity on climate. *Nature*, *326*, 483–485. doi: 10.1038/326483a0

Emanuel, Ravela, S., Vivant, E., & Risi, C. (2006). A statistical deterministic approach to hurricane risk assessment. *Bulletin of the American Meteorological Society*, *87*(3), 299–314. Retrieved from `https://doi.org/10.1175/BAMS-87-3-299` doi: 10.1175/BAMS-87-3-299

Emanuel, K. A. (2013). Downscaling CMIP5 climate models shows increased tropical cyclone activity over the 21st century. *Proceedings of the National Academy of Sciences*, *110*, 12219–12224. doi: 10.1073/pnas.1301293110

Emanuel, K. A., Sundararajan, R., & Williams, J. (2008). Hurricanes and global warming: Results from downscaling IPCC AR4 simulations. *Bulletin of the American Meteorological Society*, *89*, 347–367. doi: 10.1175/BAMS-89-3-347

Erickson, N. E., & Patricola, C. M. (2023, February 16). Future projections of the El Niño–Southern Oscillation and Tropical Pacific mean state in CMIP6. *Jour-*

nal of Geophysical Research: Atmospheres, *128*(3), e2022JD037563. (Article e2022JD037563) doi: 10.1029/2022JD037563

Eyring, V., Bony, S., Meehl, G. A., Senior, C. A., Stevens, B., Stouffer, R. J., & Taylor, K. E. (2016). Overview of the coupled model intercomparison project phase 6 (CMIP6) experimental design and organization. *Geoscientific Model Development*, *9*, 1937–1958. doi: 10.5194/gmd-9-1937-2016

Fosu, B. O., et al. (2024). Assessing future tropical cyclone risk using downscaled CMIP6 projections. *Journal of Catastrophe Risk and Resilience*, *2024*(2), 1. doi: 10.63024/dpva-2pa1

Fu, D., Chang, P., Patricola, C. M., & Saravanan, R. (2019). High-resolution tropical channel model simulations of tropical cyclone climatology and intraseasonal-to-interannual variability. *Journal of Climate*, *32*, 7871–7895. doi: 10.1175/JCLI-D-19-0130.1

Goldenberg, S. B., & Shapiro, L. J. (1996). Physical mechanisms for the association of El Niño and west african rainfall with atlantic major hurricane activity. *Journal of Climate*, *9*(6), 1169–1187. Retrieved from `https://doi.org/10.1175/1520-0442(1996)009<1169:PMFTAO>2.0.CO;2` doi: 10.1175/1520-0442(1996)009⟨1169:PMFTAO⟩2.0.CO;2

Gray, W. M. (1968, October 1). Global view of the origin of tropical disturbances and storms. *Monthly Weather Review*, *96*(10), 669–700. (Print publication: 1 October 1968) doi: 10.1175/1520-0493(1968)096⟨0669:GVOTOO⟩2.0.CO;2

Gray, W. M. (1984). Atlantic seasonal hurricane frequency. Part I: El Niño and 30 mb quasi-biennial oscillation influences. *Monthly Weather Review*, *112*(9), 1649–1668. doi: 10.1175/1520-0493(1984)112⟨1649:ASHFPI⟩2.0.CO;2

Hemmati, M., Lee, C.-Y., Mandli, K. T., Sobel, A. H., Camargo, S. J., & Sustiel, J. (2025, October 6). Assessment of Caribbean coastal hazard posed by tropical cyclones. *Journal of Applied Meteorology and Climatology*, *64*(11), 1681–1694. doi: 10.1175/JAMC-D-24-0123.1

Hersbach, H., et al. (2020). The ERA5 global reanalysis. *Quarterly Journal of the Royal Meteorological Society*, *146*, 1999–2049. doi: 10.1002/qj.3803

Holland, G. J. (1983). Tropical cyclone motion: Environmental interaction plus a beta effect. *Journal of the Atmospheric Sciences*, *40*(2), 328–342. doi: 10.1175/1520-0469(1983)040⟨0328:TCMEIP⟩2.0.CO;2

Jewson, S. (2024). Projecting future tropical cyclone frequencies by combining uncertain empirical estimates of baseline frequencies with climate model estimates of change. *Journal of Catastrophe Risk and Resilience*, *02*(3). doi: 10.63024/m9wk-3420

Jing, R., & Lin, N. (2020). An environment-dependent probabilistic tropical cyclone model. *Journal of Advances in Modeling Earth Systems*, *12*(4), e2019MS001975. doi: 10.1029/2019MS001975

Jones, C. G., & Thorncroft, C. D. (1998). The rôle of el niño in atlantic tropical cyclone activity. *Weather*, *53*(9), 324-336. Retrieved from `https://rmets.onlinelibrary.wiley.com/doi/abs/10.1002/j.1477-8696.1998.tb06409.x` doi: https://doi.org/10.1002/j.1477-8696.1998.tb06409.x

Kelley, M., et al. (2020). GISS-E2.1: Configurations and climatology. *Journal of Advances in Modeling Earth Systems*, *12*, e2019MS002025. doi: 10.1029/2019MS002025

Kelso, N. V., & Patterson, T. (2010). Introducing natural earth data-naturalearthdata.com. *Geographia Technica*, *5*, 82–89.

Klotzbach, P. J. (2011). The influence of El Niño–Southern Oscillation and the Atlantic Multidecadal Oscillation on Caribbean tropical cyclone activity. *Journal of Climate*, *24*(3), 721–731. Retrieved from `https://doi.org/10.1175/2010JCLI3705.1` doi: 10.1175/2010JCLI3705.1

Knapp, K. R., Diamond, H. J., Kossin, J. P., Kruk, M. C., & Schreck, C. J. I. (2018). International best track archive for climate stewardship (IBTrACS)

project, version 4. (Accessed 16 July 2024) doi: 10.25921/82TY-9E16

Knapp, K. R., Kruk, M. C., Levinson, D. H., Diamond, H. J., & Neumann, C. J. (2010). The international best track archive for climate stewardship (IBTrACS): Unifying tropical cyclone data. *Bulletin of the American Meteorological Society*, *91*, 363–376. doi: 10.1175/2009BAMS2755.1

Knutson, T. R., Camargo, S. J., Chan, J. C. L., Emanuel, K., Ho, C.-H., Kossin, J., ... Wu, L. (2020). Tropical cyclones and climate change assessment: Part II: Projected response to anthropogenic warming. *Bulletin of the American Meteorological Society*, *101*, E303–E322. doi: 10.1175/BAMS-D-18-0194.1

Knutson, T. R., McBride, J., & Chan, J. (2010). Tropical cyclones and climate change. *Nature Geoscience*, *3*, 157–163. doi: 10.1038/ngeo779

Knutson, T. R., Sirutis, J. J., Vecchi, G. A., Garner, S., Zhao, M., Kim, H.-S., ... Villarini, G. (2013). Dynamical downscaling projections of twenty-first-century atlantic hurricane activity: CMIP3 and CMIP5 model-based scenarios. *Journal of Climate*, *26*(17), 6591–6617. doi: 10.1175/JCLI-D-12-00539.1

Knutson, T. R., Sirutis, J. J., Zhao, M., Tuleya, R. E., Bender, M., Vecchi, G. A., ... Chavas, D. (2015, September 11). Global projections of intense tropical cyclone activity for the late twenty-first century from dynamical downscaling of CMIP5/RCP4.5 scenarios. *Journal of Climate*, *28*(18), 7203–7224. (Published online: 11 September 2015) doi: 10.1175/JCLI-D-15-0129.1

Kossin, J. P., Camargo, S. J., & Sitkowski, M. (2010). Climate modulation of North Atlantic hurricane tracks. *Journal of Climate*, *23*, 3057–3076. doi: 10.1175/2010JCLI3497.1

Landsea, C. W., Pielke, R. A., Mestas-Nuñez, A. M., & Knaff, J. A. (1999, May). Atlantic basin hurricanes: Indices of climatic changes. *Climatic Change*, *42*(1), 89–129. (Published: 25 May 1999) doi: 10.1023/A:1005416332322

Lee, Camargo, S. J., Sobel, A. H., & Tippett, M. K. (2020). Statistical–dynamical downscaling projections of tropical cyclone activity in a warming climate: Two diverging genesis scenarios. *Journal of Climate*, *33*, 4815–4834. doi: 10.1175/JCLI-D-19-0452.1

Lee, Tippett, M. K., Camargo, S. J., & Sobel, A. H. (2015). Probabilistic multiple linear regression modeling for tropical cyclone intensity. *Monthly Weather Review*, *143*, 933–954. doi: 10.1175/MWR-D-14-00171.1

Lee, Tippett, M. K., Sobel, A. H., & Camargo, S. J. (2016). Autoregressive modeling for tropical cyclone intensity climatology. *Journal of Climate*, *29*, 7815–7830. doi: 10.1175/JCLI-D-15-0909.1

Lee, Tippett, M. K., Sobel, A. H., & Camargo, S. J. (2018). An environmentally forced tropical cyclone hazard model. *Journal of Advances in Modeling Earth Systems*, *10*, 223–241. doi: 10.1002/2017MS001186

Lin, N., & Emanuel, K. (2016, January). Grey swan tropical cyclones. *Nature Climate Change*, *6*, 106–111. Retrieved from `https://doi.org/10.1038/nclimate2777` doi: 10.1038/nclimate2777

Meiler, S., Lee, C.-Y., Camargo, S. J., et al. (2026). Global coastal wind hazard maps from the CHAZ tropical cyclone model. *Scientific Data*, *13*(1), 136. (Article number 136) doi: 10.1038/s41597-025-06452-0

Meiler, S., Vogt, T., Bloemendaal, N., Ciullo, A., Lee, C.-Y., Camargo, S. J., ... Bresch, D. N. (2022). Intercomparison of regional loss estimates from global synthetic tropical cyclone models. *Nature Communications*, *13*, 6156. doi: 10.1038/s41467-022-33918-1

Murakami, H., & Wang, B. (2010). Future change of North Atlantic tropical cyclone tracks: Projection by a 20-km-mesh global atmospheric model. *Journal of Climate*, *23*(10), 2699–2721. doi: 10.1175/2010JCLI3338.1

Müller, W. A., et al. (2018). A higher-resolution version of the Max Planck Institute earth system model (MPI-ESM1.2-HR). *Journal of Advances in Modeling*

Earth Systems, *10*, 1383–1413. doi: 10.1029/2017MS001217

Nakamura, J., Camargo, S. J., Sobel, A. H., Emanuel, K. A., Kumar, A., LaRow, T. E., et al. (2017). Western North Pacific tropical cyclone model tracks in present and future climates. *Journal of Geophysical Research: Atmospheres*, *122*, 9721–9744. doi: 10.1002/2017JD027007

Nakamura, J., Lall, U., Kushnir, Y., & Camargo, S. J. (2009). Classifying North Atlantic tropical cyclone tracks by their mass moments. *Journal of Climate*, *22*(20), 5481–5494. doi: 10.1175/2009JCLI2839.1

O'Neill, B. C., Kriegler, E., Ebi, K. L., Kemp-Benedict, E., Riahi, K., Rothman, D. S., ... Solecki, W. (2017). The roads ahead: Narratives for shared socioeconomic pathways describing world futures in the 21st century. *Global Environmental Change*, *42*, 169-180. Retrieved from `https://www.sciencedirect.com/science/article/pii/S0959378015000060` doi: https://doi.org/10.1016/j.gloenvcha.2015.01.004

Patricola, C. M., Saravanan, R., & Chang, P. (2014). The impact of the El Niño–Southern Oscillation and Atlantic Meridional Mode on seasonal atlantic tropical cyclone activity. *Journal of Climate*, *27*, 5311–5328. doi: 10.1175/JCLI-D-13-00687.1

Patricola, C. M., Saravanan, R., & Chang, P. (2017). A teleconnection between atlantic sea surface temperature and eastern and central North Pacific tropical cyclones. *Geophysical Research Letters*, *44*, 1167–1174. doi: 10.1002/2016GL071965

Pielke, R. A., & Landsea, C. N. (1999). La Niña, El Niño, and Atlantic Hurricane Damages in the United States. *Bulletin of the American Meteorological Society*, *80*(10), 2027–2034. Retrieved from `https://doi.org/10.1175/1520-0477(1999)080<2027:LNAENO>2.0.CO;2` (Corrected journal title from "Bulletin America Meteorology Social") doi: 10.1175/1520-0477(1999)080⟨2027:LNAENO⟩2.0.CO;2

Riahi, K., van Vuuren, D. P., Kriegler, E., Edmonds, J., O'Neill, B. C., Fujimori, S., ... Tavoni, M. (2017). The shared socioeconomic pathways and their energy, land use, and greenhouse gas emissions implications: An overview. *Global Environmental Change*, *42*, 153-168. Retrieved from `https://www.sciencedirect.com/science/article/pii/S0959378016300681` doi: https://doi.org/10.1016/j.gloenvcha.2016.05.009

Rios-Berrios, R., Finocchio, P. M., Alland, J. J., Chen, X., Fischer, M. S., Stevenson, S. N., & Tao, D. (2024). A review of the interactions between tropical cyclones and environmental vertical wind shear. *Journal of the Atmospheric Sciences*, *81*(4), 713–741. doi: 10.1175/JAS-D-23-0022.1

Saunders, M. A., Chandler, R. E., Merchant, C. J., & Roberts, F. P. (2000). Atlantic hurricanes and NW pacific typhoons: ENSO spatial impacts on occurrence and landfall. *Geophysical Research Letters*, *27*(8), 1147–1150. doi: 10.1029/1999GL010948

Seager, R., Cane, M., Henderson, N., Lee, D.-E., Abernathey, R., & Zhang, H. (2019). Strengthening Tropical Pacific zonal sea surface temperature gradient consistent with rising greenhouse gases. *Nature Climate Change*, *9*, 517–522. doi: 10.1038/s41558-019-0505-x

Seager, R., Henderson, N., & Cane, M. (2022). Persistent discrepancies between observed and modeled trends in the Tropical Pacific ocean. *Journal of Climate*, *35*, 4571–4584. doi: 10.1175/JCLI-D-21-0648.1

Sellar, A. A., et al. (2019). UKESM1: Description and evaluation of the u.k. earth system model. *Journal of Advances in Modeling Earth Systems*, *11*, 4513–4558. doi: 10.1029/2019MS001739

Smith, S. R., Brolley, J., O'Brien, J. J., & Tartaglione, C. A. (2007). ENSO's impact on regional U.S. hurricane activity. *Journal of Climate*, *20*(7), 1404–1414. doi: 10.1175/JCLI4063.1

Sobel, A. H., Camargo, S. J., Hall, T. M., Lee, C.-Y., Tippett, M. K., & Wing, A. A. (2016). Human influence on tropical cyclone intensity. *Science*, *353*, 242–246. doi: 10.1126/science.aaf6574

Sobel, A. H., Wing, A. A., Camargo, S. J., Patricola, C. M., Vecchi, G. A., Lee, C.-Y., & Tippett, M. K. (2021). Tropical cyclone frequency. *Earth's Future*, *9*(12), e2021EF002275. doi: 10.1029/2021EF002275

Stansfield, A. M., Reed, K. A., & Zarzycki, C. M. (2020). Changes in precipitation from North Atlantic tropical cyclones under RCP scenarios in the variable-resolution Community Atmosphere Model. *Geophysical Research Letters*, *47*(4), e2019GL086930. doi: 10.1029/2019GL086930

Tang, B. H., & Neelin, J. D. (2004). ENSO influence on atlantic hurricanes via tropospheric warming. *Geophysical Research Letters*, *31*(24), L24204. doi: 10.1029/2004GL021072

Tatebe, H., et al. (2019). Description and basic evaluation of simulated mean state, internal variability, and climate sensitivity in MIROC6. *Geoscientific Model Development*, *12*, 2727–2765. doi: 10.5194/gmd-12-2727-2019

Tebaldi, C., et al. (2021). Climate model projections from the scenario model intercomparison project (ScenarioMIP) of CMIP6. *Earth System Dynamics*, *12*, 253–293. doi: 10.5194/esd-12-253-2021

Ting, M., Camargo, S. J., Li, C., & Kushnir, Y. (2015, May 15). Natural and forced North Atlantic hurricane potential intensity change in CMIP5 models. *Journal of Climate*, *28*(10), 3926–3942. doi: 10.1175/JCLI-D-14-00520.1

Ting, M., Kossin, J. P., Camargo, S. J., & Li, C. (2019). Past and future hurricane intensity change along the U.S. East Coast. *Scientific Reports*, *9*, 7795. doi: 10.1038/s41598-019-44252-w

Tippett, M. K., Camargo, S. J., & Sobel, A. H. (2011). A poisson regression index for tropical cyclone genesis and the role of large-scale vorticity in genesis. *Journal of Climate*, *24*, 2335–2357. doi: 10.1175/2010JCLI3811.1

Vecchi, G. A., Delworth, T. L., Murakami, H., Underwood, S. D., Wittenberg, A. T., Zeng, F., ... Yang, X. (2019, November). Tropical cyclone sensitivities to CO2 doubling: Roles of atmospheric resolution, synoptic variability and background climate changes. *Climate Dynamics*, *53*(9), 5999–6033. (Published: 12 August 2019) doi: 10.1007/s00382-019-04913-y

Vecchi, G. A., & Soden, B. J. (2007a). Effect of remote sea surface temperature change on tropical cyclone potential intensity. *Nature*, *450*, 1066–1070. doi: 10.1038/nature06423

Vecchi, G. A., & Soden, B. J. (2007b). Increased Tropical Atlantic wind shear in model projections of global warming. *Geophysical Research Letters*, *34*(8), L08702. doi: 10.1029/2006GL028905

Voldoire, A., et al. (2019). Evaluation of CMIP6 DECK experiments with CNRM-CM6-1. *Journal of Advances in Modeling Earth Systems*, *11*, 2177–2213. doi: 10.1029/2019MS001683

Walsh, K. J. E., et al. (2016). Tropical cyclones and climate change. *Wiley Interdisciplinary Reviews: Climate Change*, *7*, 65–89. doi: 10.1002/wcc.371

Wang, B., & Chan, J. C. L. (2002). How strong ENSO events affect tropical storm activity over the Western North Pacific. *Journal of Climate*, *15*, 1643–1658. doi: 10.1175/1520-0442(2002)015⟨1643:HSEEAT⟩2.0.CO;2

Wang, C., Deser, C., Yu, J.-Y., DiNezio, P., & Clement, A. (2017). El Niño and southern oscillation (ENSO): A review. In P. W. Glynn, D. P. Manzello, & I. C. Enochs (Eds.), *Coral reefs of the eastern tropical pacific* (Vol. 8, pp. 85–106). Springer. doi: 10.1007/978-94-017-7499-4_4

Williams, C. J. R., et al. (2021). Simulation of the mid-pliocene warm period using HadGEM3: Experimental design and results from model–model and model–data comparison. *Climate of the Past*, *17*, 2139–2163. doi: 10.5194/cp-17-2139-2021

Wills, R. C. J., Dong, Y., Proistosecu, C., Armour, K. C., & Battisti, D. S. (2022). Systematic climate model biases in the large-scale patterns of recent sea-surface temperature and sea-level pressure change. *Geophysical Research Letters*, *49*(17), e2022GL100011. (Article e2022GL100011) doi: 10.1029/2022GL100011

Yokoi, S., Takayabu, Y. N., & Murakami, H. (2013, June 15). Attribution of projected future changes in tropical cyclone passage frequency over the Western North Pacific. *Journal of Climate*, *26*(12), 4096–4111. (Published: 15 June 2013) doi: 10.1175/JCLI-D-12-00218.1

Yoshida, K., Sugi, M., Mizuta, R., Murakami, H., & Ishii, M. (2017). Future changes in tropical cyclone activity in high-resolution large-ensemble simulations. *Geophysical Research Letters*, *44*(19), 9910–9917. doi: 10.1002/2017GL075058

Yukimoto, S., et al. (2019). The meteorological research institute earth system model version 2.0, MRI-ESM2.0: Description and basic evaluation of the physical component. *Journal of the Meteorological Society of Japan*, *97*, 931–965. doi: 10.2151/jmsj.2019-051

Zarzycki, C. M., Jablonowski, C., & Taylor, M. A. (2014). Using variable-resolution meshes to model tropical cyclones in the Community Atmosphere Model. *Monthly Weather Review*, *142*, 1221–1239. doi: 10.1175/MWR-D-13-00179.1

Zhao, K., Zhao, H., Klotzbach, P. J., et al. (2026). Anthropogenic warming projected to drive a decline in global tropical cyclone frequency in CMIP6 simulations. *npj Climate and Atmospheric Science*, *9*, 58. (Article number 58) doi: 10.1038/s41612-026-01330-x

Zhuo, J. Y., Lee, C. Y., Sobel, A., Seager, R., Camargo, S. J., Lin, Y. H., ... Reed, K. A. (2025). A more La Niña-like response to radiative forcing after flux adjustment in CESM2. *Journal of Climate*, *38*(4), 1037–1050. doi: 10.1175/JCLI-D-24-0331.1

Ziehn, T., et al. (2020). The Australian earth system model: ACCESS-ESM1.5. *Journal of Southern Hemisphere Earth Systems Science*, *70*, 193–214. doi: 10.1071/ES19035